HaloSat Data Reprocessing and Calibration Updates

Jesse Bluem, Philip Kaaret, Lorella Angelini

May 2023

1 Summary

This document describes the changes in the HaloSat data reprocessing (PROCVER hsuf_20221026) for the final archive, the new arf and other calibration caveats.

The reprocessing includes various changes and error corrections, such as incorrect satellite position and velocity values, corrupted PDF summaries for select fields, a few instances of special data filtering on particular fields and a channel adjustment. The reprocessed data were delivered to the HEASARC and made publicly available. With this data reprocessing is no longer necessary to apply a gain shift during spectral fitting.

The released new ARF file (hs_sdd_all20180701v002.arf) now includes the edge, removing the need to include an edge manually during spectral fitting.

2 Reprocessing Changes

To prepare for the 2023 data reprocessing, the pipeline was moved to a new server and updated from Python 2 to Python 3. In addition to the necessary syntax changes for these updates, the following changes/bug fixes were implemented:

1. The standard screening of the HaloSat data includes a hard-rate cut at 0.16 c/s in the 3-7 keV band. Previous data processing used a higher value of the hard-rate cut for fields 84, 102, 112, 233, 275, 293, and 297 only considering early time intervals. Later observations showed that these early times had high backgrounds and the special cut rates were inappropriate for the full set of observations. The new processing applies the standard hard-rate cut also for these fields.

2. The values of the column ATT_VALID in the attitude FITS file has been set to 255 for “no info”. The previous version of the attitude file has no allowed values in the ATT_VALID column. Unfortunately, the raw telemetry also contains invalid values.

3. The alignment file is now used when the pipeline runs the ‘prefilter’ tool. Some of the columns in the output of prefilter are added in the HK FITS file. The alignment file improves the accuracy of the right ascension and declination, as well as roll, for the spacecraft.

4. In the HK FITS file the POSITION and VELOCITY were incorrectly formatted. This bug has been fixed.

5. A bug fix corrected a channel offset present in data processed with older versions of the pipeline. The offset required a gain shift in spectral fitting. With the new data the gain shift is no longer necessary (see Gain correction section).

6. The header keywords DATE-OBS and DATE-END were changed from TAI time to UTC by adding 32 seconds.

7. Corrupted PDF summary files were fixed. The previous pipeline version produced incorrect PDF files for two reasons. The first issue affected the dark Earth fields 1044, 1047, 1048, and 1049, which were missing from an original list of targets, which triggered an exit condition in the code during PDF writing. The second issue affected fields 27, 134, 147, 151, 347, where the standard Sun angle selection produced 0 length GTIs and caused an error when writing the PDF.

8. A general fix to all PDFs was to change the Y-axis of plots to be dynamic based on the count rate of the particular field. This prevented plots from being cut off in high-rate fields.

3 Gain correction

The HaloSat data available at the HEASARC archive since May 1st 2023, PROCVER hsuf_20221026, do not require gain shift in the spectral fitting. Data downloaded from the archive prior to May 1st 2023, with processing version, PROCVER hsuf_20200226, requires the gain shift to be applied in the spectral fitting.

The bug in the PROCVER hsuf_20200226 resulted in a channel shift of 1 being applied to the spectra, which accounted for most of the original fitted gain. The remaining portion of the originally suggested gain is no longer recommended for any data release.

The gain shift was derived from an examination of spectra obtained while observing the supernova remnant (SNR) Cassiopeia A (Cas A, Bluem et al. (2022), appendix). Cas A was selected as a calibration target due to the strong emission lines present in its X-ray spectrum (Holt et al. 1994; Jahoda et al. 2006). The HaloSat field centered on Cas A includes another SNR, CTB 109, but Cas A dominates the emission.

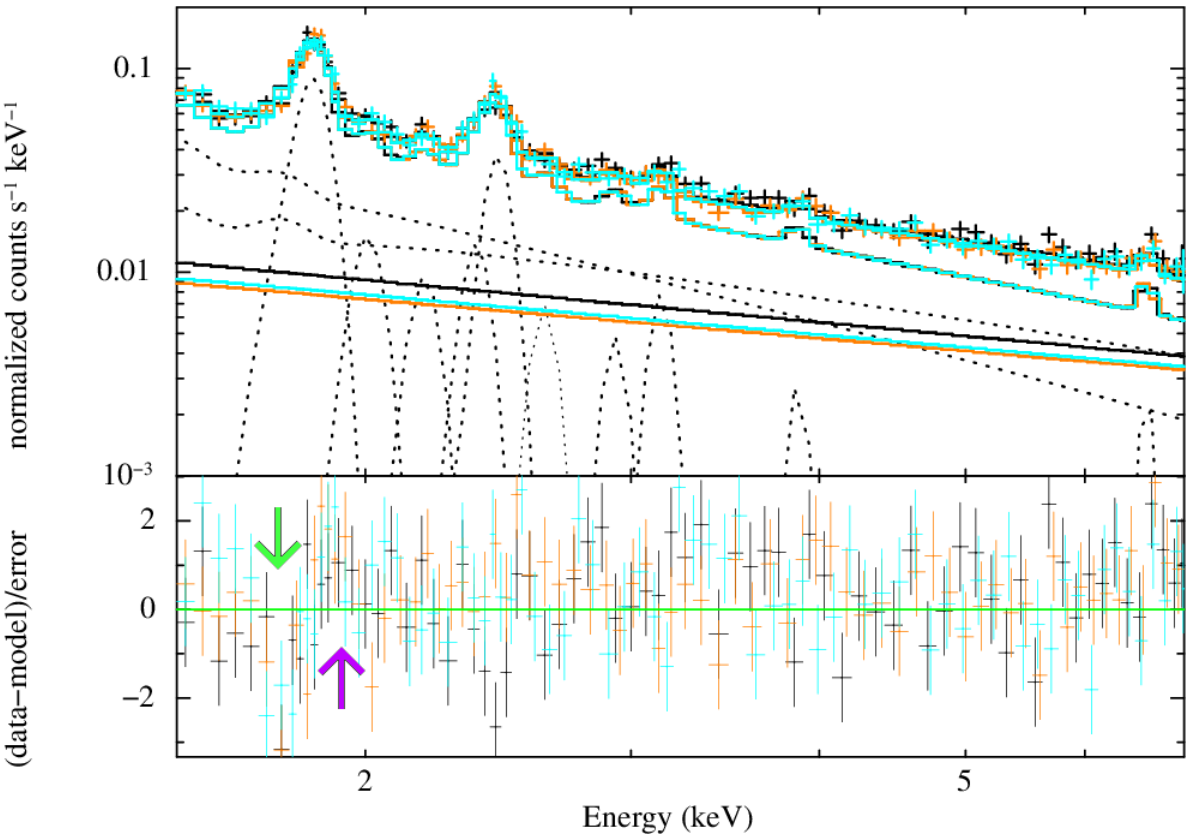

Figure 1: Cas A spectral model with a single Si XIII Gaussian line at a fixed energy. The full energy range fit is 1.5-7 keV. The green arrow marks a concerning feature associated with the Si XIII Gaussian line, which is near the Si Edge added to our response. The purple arrow marks a small secondary residual feature associated with the same Gaussian line.

While most of the original gain shift was removed by the aforementioned bug fix, a small portion remained. As such, the newly reprocessed Cas A spectra were reanalyzed to test the need of any remaining gain shift. The preliminary Cas A spectral fits a range of 1.5-7 keV. (Figure 1) exhibited a feature in the residuals that coincided with the location of both a prominent spectral line (Si XIII) and the silicon absorption edge (see section 4). However, this feature only appears in the Cas A spectrum and cannot be explained by any further adjustments to the edge model, which would affect all observed targets. Such a significant residual feature associated with a spectral line is a cause for concern when attempting to calibrate the on-orbit X-ray energy scale.

Since the residual feature of interest is associated with a spectral line (and may include a subtle counterpart residual on the other side of the line, Figure 1) it is possible that the line energy may need to be adjusted. The original line was fixed at 1.8558 keV, but this line is actually the SI XIII triplet.

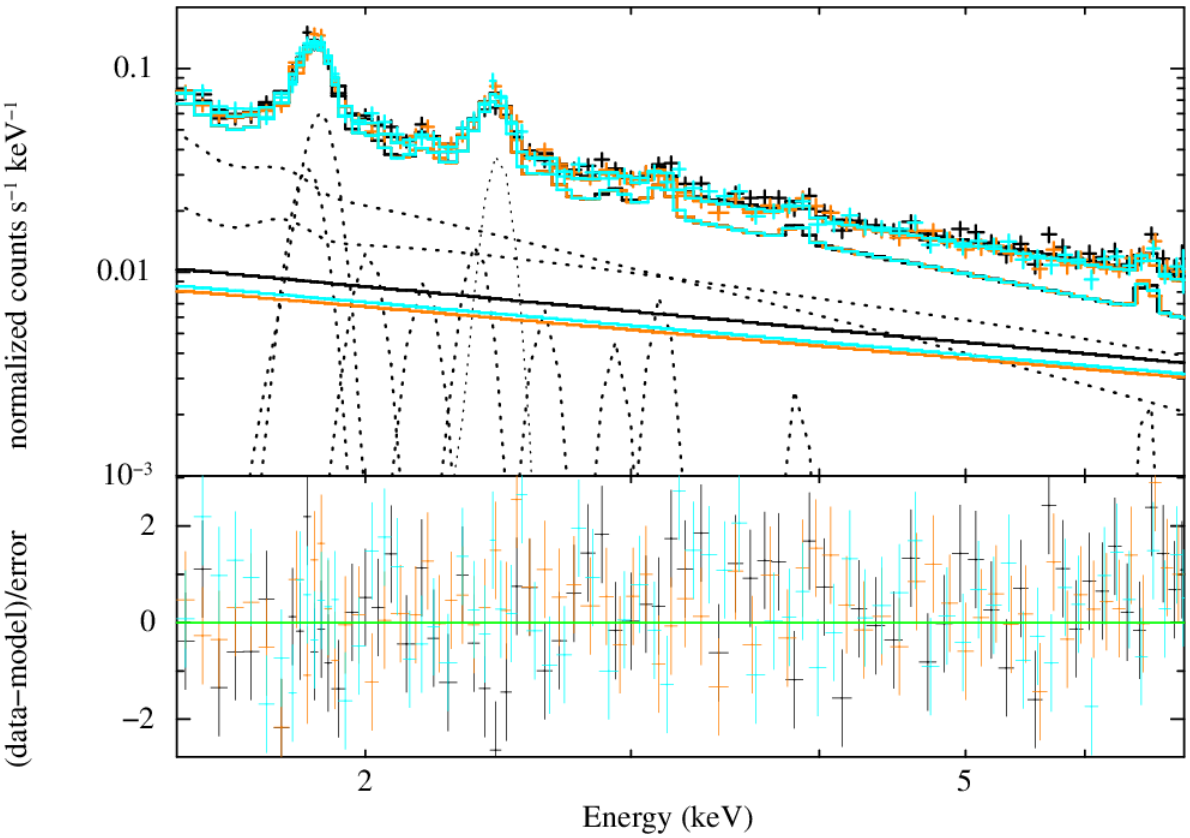

Figure 2: Cas A spectral model (1.5-7 keV) with the Si XIII Gaussian line split into two components with fixed energies. The residuals and fit statistics are improved when compared to Figure 1.

An improvement to the spectral fit (from a χ^2/DoF of 939.9/806 = 1.17 to 894.6/805 = 1.11, Figure 2) can be achieved by fitting to the two strongest Si XIII lines on AtomDB at 1.865 keV and 1.839 keV. Those lines are listed with relative intensities of 1 and 0.53 on AtomDB, while the Gaussians fit to relative strengths of 1 and 0.47. The third line in the triplet is at 1.854 keV with a relative strength of 0.17, and was not used in the fit. Similar analysis was initially performed over a range of 1.2-7 keV, but the slightly larger energy range exhibited issues with the model fitting that implies an unfit or ill-fit power law component (or some type of other broad component) contributing at the low energies. While residual features remained in the fit with this wider energy range, the double fixed Gaussian model was a significant improvement. The gain can be fit for either model over the 1.5-7 keV range. The results can be seen in Table 1.

Model	D14 gain offset	D54 gain offset	D38 gain offset
Single line	$0.0037^{+0.0006}_{-0.0010}$	$0.0042^{+0.0005}_{-0.0006}$	$0.0044^{+0.0006}_{-0.0005}$
Double line	$-0.0039^{+0.0029}_{-0.0011}$	$0.002^{+0.016}_{-0.002}$	$0.0004^{+0.0026}_{-0.0047}$

Table 1: A comparison of the fitted gain offsets (in keV) for each HaloSat detector using different Cas A model fits. The first row models the Si XIII line as a single Gaussian at 1.8558 keV. The second row splits that line into two Gaussian components at 1.839 keV and 1.865 keV. The values found for gain depend heavily on how this single Gaussian feature is handled in the model fit and is sometimes consistent with zero. As such, we do not recommend the inclusion of any gain parameters in the reprocessed data archive (PROCVER hsuf_20221026).

Many of these new gain parameters are consistent with zero, and all are inconsistent with the remainder of the gain from the original Cas A analysis (Bluem et al. 2022, appendix). Thus, it appears that the gain was incorrectly derived from a residual feature caused by a complicated spectral line. At a minimum, the remainder of the original gain fit is thrown in doubt due to how dependent fitting the gain is on that single spectral feature. As such, we no longer recommend including any gain shift when fitting HaloSat spectra from the new data archive. Data downloaded before May 2023 date (PROCVER hsuf_20200226) should still include a gain shift as described in Bluem et al. (2022). However, the gain offsets can be reasonably truncated to 0.02 keV for all 3 detectors.

4 Flight Calibration of the ARF

This section describes the inflight calibration of the original edge analysis from Bluem et al. (2022). The edge feature has been re-verified using the reprocessed data archive, and the edge has been integrated into the HaloSat ARF (hs_sdd_all20180701v002.arf).

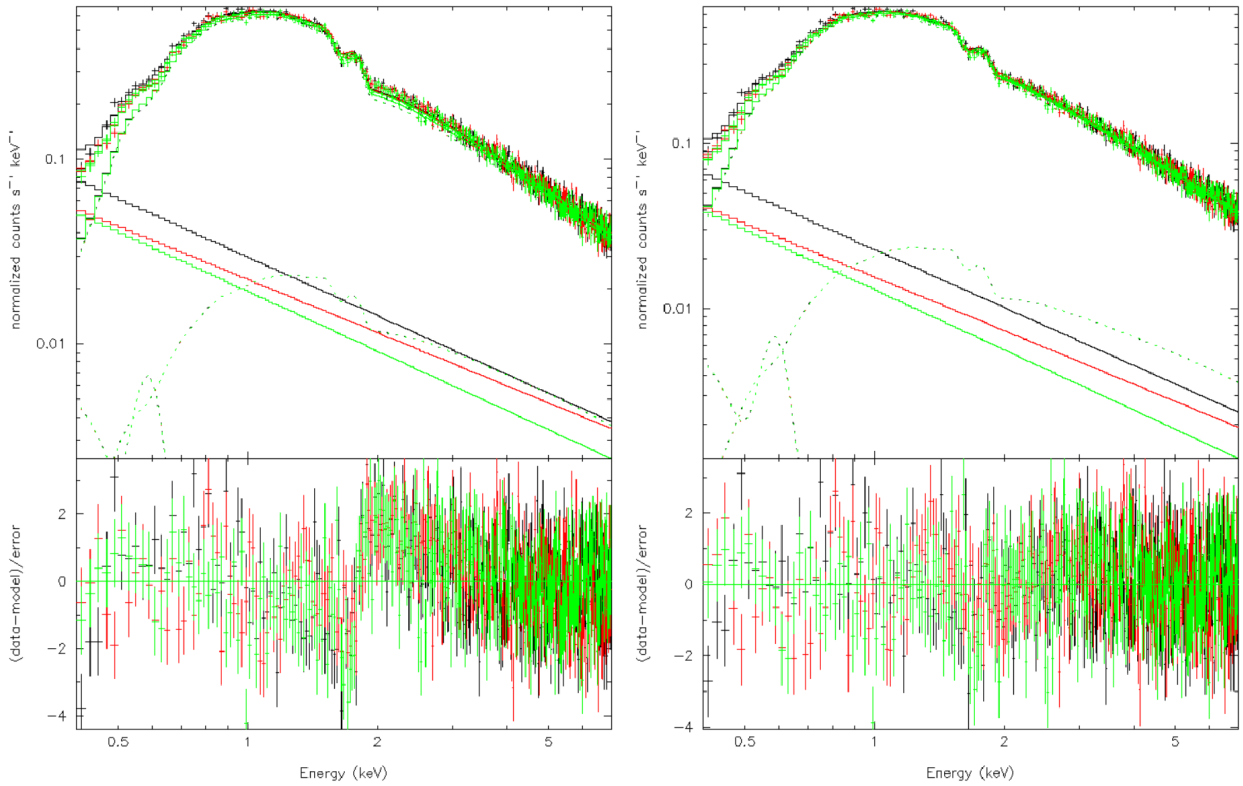

Figure 3: Crab spectrum before (left) and after (right) the inclusion of the negative Si edge. There are initially strong residuals around 1.8 keV. After the inclusion of a negative edge Si edge, the residuals around 1.8 keV are greatly improved.

The inflight calibration analyzed all the HaloSat observations of the Crab pulsar wind nebula and pulsar data to determine the parameter associated to the edge (Bluem et al. 2022). The Crab is chosen for this purpose because it has a featureless X-ray spectrum and the emission within the HaloSat field centered on the Crab is dominated by the Crab. Data (PROCVER hsuf_20200226) were filtered using selections on the VLE (> 7 keV) count rate of 0.75 c/s and on the hard band (3-7 keV) count rate of 0.5 c/s. A Sun angle greater than 100^{o} was required. The count rate threshold in the hard band is higher than typically used in HaloSat analysis because the Crab contributes significant flux in the hard band. Figure 3 shows one summed spectrum for each of the three DPUs with channels grouped to have a minimum of 25 counts per bin. The gain corrections described in the previous section were applied. The instrumental background was modelled as a power law with a diagonal response matrix. The normalization and photon index for each DPU were left as free parameters. The instrumental background photon index calculation described in Kaaret et al. (2020) is not applicable due to the non-standard data filtering required for the Crab. Emission from the cosmic X-ray background (CXB) was modeled as an absorbed power law with fixed absorption, photon index, and normalization. Emission from the local hot bubble (LHB) was modeled as an unabsorbed APEC. The parameters for the CXB and

LHB were set following Kaaret et al. (2020). The emission from the Crab was modeled as an absorbed power law. The absorption column density and power law photon index and normalization were allowed to vary. Figure 3 (left) shows the spectra for all three detectors. The spectral fits show strong residuals near 1.8 keV which we identify as the silicon K edge. The fit has χ^2/DoF = 1424.38/978. Figure 3 (right) also shows the spectral fits including an edge (model 'edge' in Xspec) with the edge energy fixed to 1.839 keV for silicon. The maximum optical depth (tau) is linked between the detectors and the best fit value is tau = -0.169 ± 0.014. Addition of the edge significantly improves the fit to χ^2/DoF = 1084.85/977. The corresponding F-test probability is $9x10^{-60}$. Allowing tau to vary between detectors produces no significant improvement in the fit (F-test probability = 0.38). The error ranges on the tau values for the individual detectors all include the linked fit value of tau = -0.169.

When fitting the data with the ARF file hs_sdd_all20180701v001.arf it is recommended to include a negative absorption edge to model this feature. Using Xspec, this is an edge model with a threshold energy of 1.839 keV and tau of -0.169 in all model fits. The edge is 'negative' implying that there is less absorption of that included in the ARF file hs_sdd_all20180701v001.arf.

The edge model spectral fit was verified also with the Crab spectral files obtained with the reprocessed data (PROCVER hsuf_20221026). The parameters of edge model are consistent with the original analysis.

A Si thickness of 0.24 microns produces a step in transmission across the Si K edge equivalent to the measured tau. Such a change in Si thickness should also affect the transmission at low energies, but this is not observed. The equivalent Si thickness is comparable to the thickness of the front layer (0.11 microns) and the incomplete charge collection layer (0.20 microns) of the HaloSat silicon drift detectors (Zajczyk et al. 2020). The edge may result from incomplete modeling of the interactions of the Auger and photo-electrons in those regions (Scholze & Procop 2009).

Since the edge model is also needed to fit the reprocessed data, the ARF was modified to include the edge using the parameters derived in the Bluem et al. 2022 appendix. The edge model was calculated for each bin in the ARF above the threshold energy (Ec) of 1.839 keV, based on the lower edge of the bin's energy range (E), using the mathematical definition of the XSPEC edge model $e^{-D(E/Ec)^{-3}}$ with a D=-0.17. The effect of the edge has been included in the HaloSat ARF file hs_sdd_all20180701v002.arf and released together with the new reprocessed data.

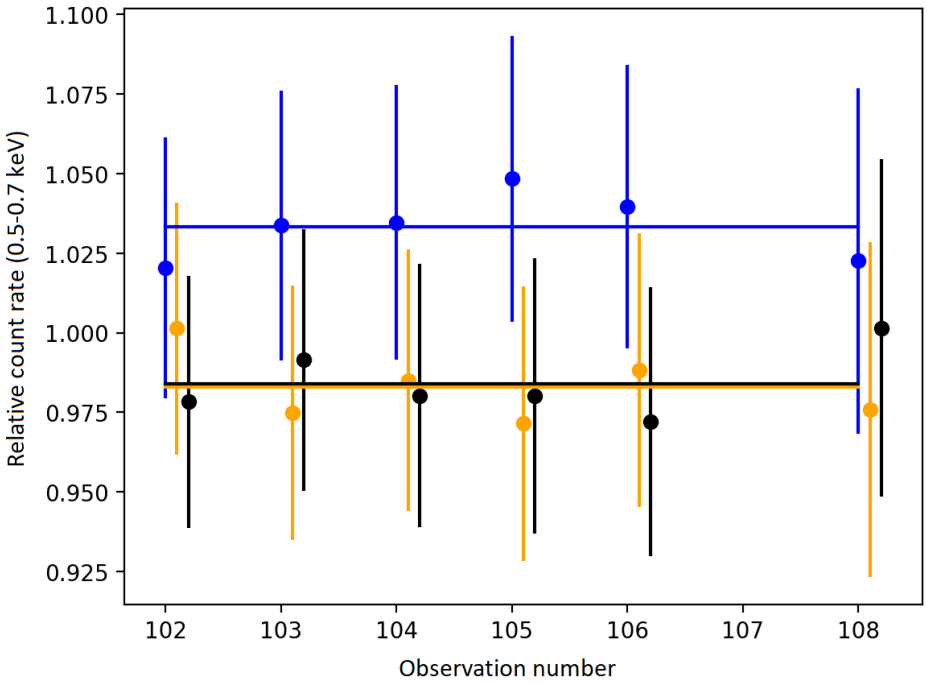

Figure 4: A comparison of the relative count rates for DPU 14 (blue) versus DPUs 38 and 54 (orange and black) for individual observations of the Cygnus Loop, over a range of 0.5-0.7 keV. A similar enhancement is seen throughout the circumgalactic medium data set from Bluem et al. (2022), with DPU 14 consistently exhibiting this small enhancement only in this energy range.

Previous work with HaloSat data has pointed towards a potential count rate enhancement in detector 14 over a range of roughly 0.5-0.7 keV (Figure 4). This enhancement is small and not statistically significant in terms of error, however, it is persistently seen throughout the HaloSat data set. Attempts to explain it in terms of the tunable physical parameters of the detector ARF yielded no results. Adjustments to the active and dead layers of the detector were unable to explain the enhancement. The instrument's collimator is effectively opaque. The detector window has a nearby nitrogen feature, but it lies outside the energy band of interest.

Bluem et al 2022, ApJ 936, 72B, 17 pp.
Holt et al 1994, PASJ 46, L151 p.
Jahoda et al 2006, ApJS 163, 401 pp.
Kaaret et al 2020, NatAs 4, 1072 p.
Scholze & Procop 2009, XRS 38, 312 pp.
Zajczyk et al 2020, JATIS 6, 044005